

Temporal Triplane Transformers as Occupancy World Models

Haoran Xu^{1,2}, Peixi Peng^{2,3†}, Guang Tan^{1†}, Yiqian Chang^{2,4}, Yisen Zhao³, and Yonghong Tian^{2,3,5}

¹ School of Intelligent Systems Engineering, Shenzhen Campus of Sun Yat-sen University

² Peng Cheng Laboratory

³ School of Electronic and Computer Engineering, Shenzhen Graduate School, Peking University

⁴ School of Computer Science and Technology, Harbin Institute of Technology

⁵ School of Computer Science, Peking University

Abstract

World models aim to learn or construct representations of the environment that enable the prediction of future scenes, thereby supporting intelligent motion planning. However, existing models often struggle to produce fine-grained predictions and to operate in real time. In this work, we propose T³Former, a novel 4D occupancy world model for autonomous driving. T³Former begins by pre-training a compact *triplane* representation that efficiently encodes 3D occupancy. It then extracts multi-scale temporal motion features from historical triplanes and employs an autoregressive approach to iteratively predict future triplane changes. Finally, these triplane changes are combined with previous states to decode future occupancy and ego-motion trajectories. Experimental results show that T³Former achieves $1.44\times$ speedup (26 FPS), improves mean IoU to 36.09, and reduces mean absolute planning error to 1.0 meters. Demos are available in the supplementary material.

1 Introduction

World models [10, 9] aim to represent the environment, predict future scenes and enable agents to perform advanced motion planning. These models first encode sensory inputs into compact, lower-dimensional representations, which are then used to model the temporal evolution of the environment. When applied to autonomous driving [58, 46, 51, 16, 8, 53], world models help anticipate potential hazards and support more informed, safer decision-making [6].

Existing models [14, 16, 19, 57] focus on predicting future instance segmentation of traffic participants from a Bird’s Eye View (BEV), or use diffusion models [48, 45, 44, 7, 18] to generate future driving scenes. However, these approaches encounter challenges in establishing fine-grained, 3D associations between scene changes and the agent’s motion planning. Recently, 3D occupancy [40, 32, 39, 47, 28] has emerged as a structured and spatially rich representation of the environment. It enables finer correlations between occupied voxels and planning decisions, thus offering improved support for downstream control tasks. In this paper, we focus on the design of Occupancy World Models (OWMs) to address this challenge.

In this context, the first task is to learn a compact representation of the raw occupancy data [46, 58, 51], which must preserve both geometric and semantic details. Current methods mainly employ VQ-VAE [41, 24] for the purpose. While VQ-VAE has shown success in several generative tasks [35, 20, 55], its application to compressing occupancy data forces the latent space of 3D structures to be discretized. This results in different 3D structures sharing the same token in the codebook, inevitably causing a loss of 3D structural features and reduced accuracy. Furthermore, in real-world scenarios, most voxels in the occupancy data are empty (unoccupied) [43], and some objects contain only a

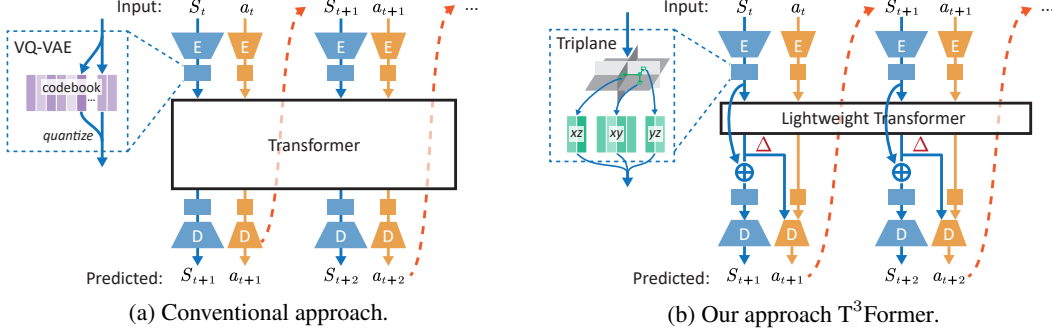


Figure 1: Different occupancy world architectures: Conventional approaches [58, 46, 51, 53, 8], as shown in (a), use a pre-trained VAE [41, 24] to compress occupancy data (denoted by S) into a compact representation code, which is then combined with encoded previous actions (marked as a) to predict future codes and actions through the Transformer. In contrast, our method, T^3 Former, shown in (b), employs more precise and efficient *triplane* representations and leverages a *lightweight* Transformer model to separately predict the triplane changes of each plane (Δ). These Δ values are then used for occupancy forecasting and motion planning.

small number of semantic voxels (e.g., pedestrians, road signs). This leads to the omission of sparse but critical details in the compressed features.

Based on the scene representation, recent world models [51, 46] often use Transformers for future state prediction. A key challenge here is capturing the diverse motion patterns of multi-scale objects on the road. For example, small objects like pedestrians or bicycles may exhibit sudden and abrupt motion changes, while larger objects such as trucks or buses tend to demonstrate more inertial movement, potentially requiring a different modeling granularity. Furthermore, they employ the Transformer to directly predict the *complete future occupancy state*. This end-to-end approach requires the model to learn both state changes and absolute state reconstruction simultaneously, increasing the learning burden. This not only demands larger model capacity but also increases the risk of error accumulation in long-term predictions.

We present a novel occupancy world model using *temporal triplane transformers*, termed T^3 Former, that addresses the aforementioned challenges. First, we propose to compress the 3D occupancy data into a *triplane* structure, a concept from computer graphics [21, 37, 15, 38, 17, 25]. A triplane comprises three planes – xy , xz , and yz – onto which the occupancy data are projected. Compared to VQ-VAE, this representation ensures high reconstruction accuracy of the occupancy grid, achieving a 20% improvement in mIoU while reducing the latent space size by 34%. Next, we extend the representation to the temporal dimension (xyt , xzt , and yzt), using Transformer models across multiple scales to regressively generate incremental changes in the triplane. Finally, we leverage these changes, along with the previous occupancy state, to predict future occupancy and perform motion planning.

Compared to conventional approaches, we focus on predicting occupancy state changes across varying scales within the triplane space, which more effectively capture environmental dynamics. As a result, as shown in Figure 2, T^3 Former mitigates cumulative errors in long-term occupancy predictions, leading to an 81.1% increase in averaged mIoU. Additionally, motion planning accuracy achieves the lowest average error of 1.0 meter and the lowest average collision rate of 30%. Furthermore, by leveraging the concept of Δ predictions, T^3 Former significantly reduces model capacity, achieving 26 FPS. In summary, our contributions are mainly three-fold:

- We design a novel 4D autoregressive occupancy world model, T^3 Former, that enhances long-term scene forecasting and enables precise motion planning.

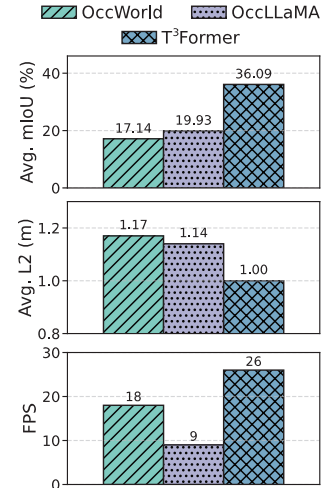


Figure 2: Performance comparisons on the test dataset. Our T^3 Former achieves more accurate occupancy forecasting and motion planning with faster inference speed.

- T³Former pre-trains a compact occupancy triplane representation to predict future incremental changes of triplanes using multi-scale Transformers. These changes, combined with the previous frame’s output, are then decoded into occupancy states and motion trajectories.
- Extensive experiments validate our state-of-the-art (SOTA) performance in terms of occupancy forecasting, motion planning, and real-time execution.

2 Related Works

3D occupancy reconstruction. 3D occupancy reconstruction techniques [40, 32, 39, 47, 28, 52] primarily utilize multi-camera RGB images or LiDAR point clouds as inputs to reconstruct the surrounding environment into an agent-centric 3D occupancy space, represented as fixed-size voxels. Each voxel contains a four-tuple attribute [40]: 3D coordinates (x , y , and z) and a semantic category. Existing methods mainly focus on how to establish precise semantic correlations between the raw sensor inputs and the 3D voxels. Once an accurate occupancy reconstruction is achieved, further learning of the temporal dynamics of scene changes becomes necessary [26].

4D occupancy prediction. To infer potential future scene changes, extensive 4D occupancy prediction approaches have been developed to learn the underlying temporal dynamics of scene evolution. Some methods [30, 33, 23] aim to predict future sensor-level data, which is then voxelized into occupancy data, while others [31, 4, 50, 49] leverage historical observations to directly predict occupancy outcomes. These methods mainly focus on reducing spatio-temporal biases on future occupancy predictions. However, they overlook the use of predicted scenes for effective and comprehensive motion planning.

World models for autonomous driving. World models [10, 9] aim to compress high-dimensional scene representations to capture the temporal dynamics of scene transitions, facilitating both future scene predictions and motion planning for the agent. In autonomous driving, existing models [14, 16, 19, 57] typically map surrounding traffic participants to the BEV perspective to predict instance-level tracklets or directly use diffusion models [48, 45, 44, 7, 18] to generate pixel-level future driving views. These methods derive control signals for the agent from current observations and predicted surroundings, but they rely solely on 2D BEV or image space, which limits the ability to establish fine-grained, efficient correlations between scene changes and motion planning. Recent world models [46, 51, 58] have leveraged 3D occupancy data to address this issue. However, they typically use VAE-series [41] models for environment compression, which often neglect original 3D geometric information and compromises reconstruction accuracy. Additionally, they rely on Transformers [42] to forecast the entire future scene instead of incremental changes, leading to significant error accumulation.

3 Methodology

3.1 Formulation

Next, we provide the formulation of Occupancy World Model (OWM) [58]. OWM primarily receives a sequence of scene representations and motion actions from past τ_p frames up to the current timestep t , such that $S^t \in \mathbb{R}^{H \times W \times L}$ represents the occupancy data of the agent-centric surrounding environment, with H , W , and L denoting the height, width, and length, respectively, and $a^t \in \mathbb{R}^2$ denotes a transition-related motion command. The goal of OWM is to establish a stochastic mapping, Φ , that associates past occupancy data and actions with future τ_f frames of occupancy data and action proposals. Formally:

$$S^{t:t+\tau_f}, a^{t:t+\tau_f} = \Phi(S^{t-\tau_p:t}, a^{t-\tau_p:t}). \quad (1)$$

To achieve this, we first pretrain a compressed latent representation of raw occupancy data using an Auto-encoder framework. The encoder and decoder models have parameters Φ_{enc} and Φ_{dec} , respectively. Thus, we have:

$$s^t = \Phi_{enc}(S^t), \quad \hat{S}^t = \Phi_{dec}(s^t). \quad (2)$$

where s^t and \hat{S}^t represent the latent representation and the corresponding reconstructed occupancy data, respectively.

Once we obtain the latent scene representations, we can predict future latent states with incremental changes Δs^{t+1} . These changes can be aggregated with the data from previous frames and decoded back into occupancy outcomes:

$$\Delta s^{t+1}, s^{t+1} = \Phi_{fut}(s^{t-\tau_p:t}), \hat{X}^{t+1} = \Phi_{dec}(s^{t+1}). \quad (3)$$

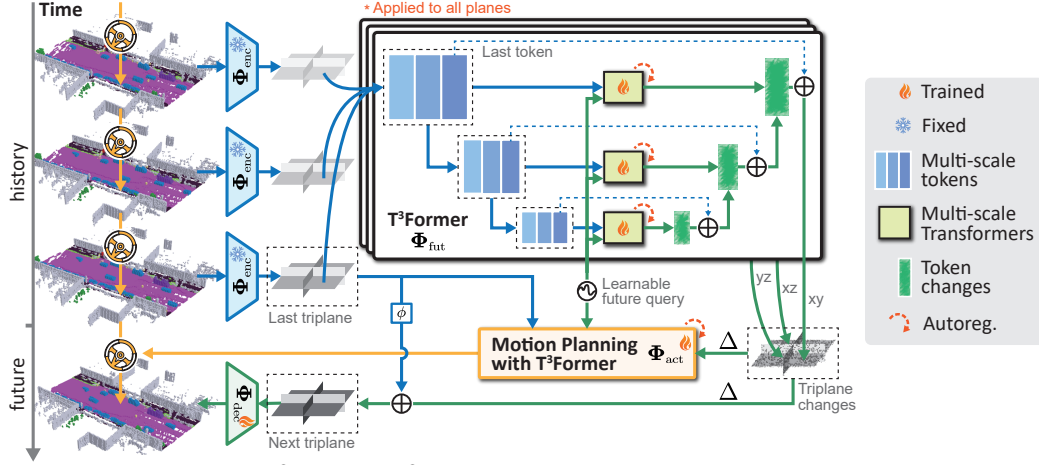


Figure 3: Workflow of T³Former. T³Former first pre-trains compact triplane representations of occupancy data. Next, T³Former utilizes multi-scale Transformers to capture comprehensive temporal dynamics within each plane, thereby predicting future triplane changes. Finally, T³Former leverages these predicted changes, along with the previous triplane, to generate future motion proposals.

Next, we utilize the incremental latent changes, along with the latent states before the change, and the historical actions, to generate future transitions as follows:

$$a^{t+1} = \Phi_{\text{act}}(a^{t-\tau_p:t}, s^t, \Delta s^{t+1}). \quad (4)$$

Note that our OWM, $\Phi = \{\Phi_{\text{enc}}, \Phi_{\text{dec}}, \Phi_{\text{fut}}, \Phi_{\text{act}}\}$, operates in an autoregressive fashion. In particular, Eqs. (3) and (4) iteratively use previously predicted outcomes as part of the historical data to forecast future scenes and provide motion proposals. Figure 3 illustrates our design, detailed below.

3.2 T³Former as OWM

3.2.1 Pre-training triplane representations for OWM

To enable faster and more accurate predictions of future scenes $X^{t:t+\tau_f}$ by OWM, it is essential to compress the high-dimensional voxelized occupancy scene with high reconstruction accuracy. To achieve this, we employ the Triplane technique [25], which is widely used in volume rendering [21, 37, 15, 38, 17], to compress raw occupancy data in an orthogonal decomposition fashion.

Specifically, as shown in Figure 4, the occupancy data S^t is first encoded by Φ_{enc} to produce $s^t \in \mathbb{R}^{C_s \times H_s \times W_s \times L_s}$. Then, an axis-wise average pooling operation is applied to obtain three orthogonal feature planes, $s^t = [s_{xy}^t, s_{xz}^t, s_{yz}^t]$, where $s_{xy}^t \in \mathbb{R}^{C_s \times W_s \times L_s}$, $s_{xz}^t \in \mathbb{R}^{C_s \times H_s \times W_s}$, and $s_{yz}^t \in \mathbb{R}^{C_s \times H_s \times L_s}$, corresponding to the xy , xz , and yz planes, respectively. To decode the original occupancy data, for each point in the 3D occupancy grid, denoted as $pos = (x, y, z)$, it serves as a position query to retrieve the corresponding features from the three planes in s^t . These features are then summed and concatenated with the positional encoding $\text{PE}(pos)$, which is passed into Φ_{dec} to predict the semantic label for the position pos . The detailed structures of Φ_{enc} and Φ_{dec} are given in the supplementary material.

By pretraining Φ_{enc} and Φ_{dec} with Eq. (5), we obtain a highly generalizable and accurate triplane representation:

$$J_{\text{enc,dec}} = \mathbb{E}_{t \sim \mathcal{T}, pos \sim S^t} [\mathcal{L}_{\text{occ}}(\Phi_{\text{dec}}(\Phi_{\text{enc}}(S^t)), S^t)], \quad (5)$$

where \mathcal{T} represents the collection of all timesteps in the occupancy dataset, and $\mathcal{L}_{\text{occ}} = \mathcal{L}_{\text{ce}} + \lambda \mathcal{L}_{\text{lz}}$. Here, \mathcal{L}_{ce} and \mathcal{L}_{lz} denote the cross-entropy and Lovasz-softmax losses [1, 25], receptively, and λ is the trade-off factor.

The triplane representation, compared to the tokens generated by the VQ-VAE in OccWorld [58] and the MS-VAE in OccLLM [51], retains 3D structural information while achieving a more compact

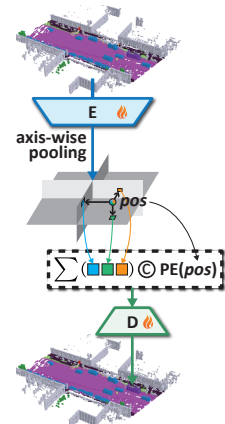


Figure 4: Pretrained triplane for OWM.

latent space. This not only makes our OWM more lightweight but also reduces the cumulative prediction error over time, as detailed later.

3.2.2 Multi-scale autoregressions in T³Former

Our T³Former model functions similarly to GPT-series [2, 29, 59], leveraging historical triplanes to generate future triplanes and using each predicted triplane to iteratively forecast subsequent ones. At timestep t , given the historical τ_p frames of triplanes $s^{t-\tau_p:t}$, the goal of T³Former is to capture the full temporal dynamics of the scene, particularly adapting to the motion patterns of objects of varying sizes. To achieve this, T³Former follows two key steps: (i) predicting each plane’s future changes, $\{\Delta s_i^{t:t+\tau_f} \mid i \in \{xy, xz, yz\}\}$, using Transformers with multiple scales; and (ii) aggregating these changes into the previous plane state and aligning the three plane predictions by fine-tuning the decoder Φ_{dec} .

In particular, $\Phi_{\text{fut}} = \{\Phi_{\text{fut}_{xy}}, \Phi_{\text{fut}_{xz}}, \Phi_{\text{fut}_{yz}}\}$. Each plane’s prediction model, Φ_{fut_i} , consists of Transformers [42] operating at multiple scales. These Transformers share the same architecture but have distinct learnable parameters and varying input sizes, depending on the plane and scale, as shown in Figure 3. For example, in the case of $\Phi_{\text{fut}_{xy}}$, the input s_{xy}^t is passed through UNet [36]-style downsampling, resulting in V scales of plane features. The feature at each scale $v \in V$ is denoted as $s_{xy}^{t,v} \in \mathbb{R}^{C_{s_{xy}}^v \times W_{s_{xy}}^v \times H_{s_{xy}}^v}$. These features are then flattened across the last two dimensions to form $W_{s_{xy}}^v \times H_{s_{xy}}^v$ tokens, which are input into the Transformer encoder to generate spatio-temporal memory. Next, we employ a learnable query $Q_{s_{xy}}^{t,v}$, which has the same dimension as $s_{xy}^{t,v}$, to enable cross-attention in the Transformer decoder and generate the token change from the current to the next time step based on the memory. Finally, the token changes at all scales are aggregated using UNet-style upsampling, yielding the plane’s feature change at the next time step, $\Delta \hat{s}_{xy}^{t+1}$. This change is then combined with the previous plane state, \hat{s}_{xy}^t , through a convolutional operation ϕ with a 1×1 kernel size.

The autoregressive forecasting process is given by:

$$\Delta \hat{s}_i^{t+k} = \Phi_{\text{fut}_i}(s_i^{t+k-\tau_p:t+k}, Q_{s_i}^{t+k}), \quad (6)$$

$$\hat{s}_i^{t+k} = \Delta \hat{s}_i^{t+k} + \phi(\hat{s}_i^{t+k-1}), \quad (7)$$

$$\hat{S}^{t+k} = \Phi_{\text{dec}}(\hat{s}^{t+k} := \{\hat{s}_i^{t+k}\}), \quad (8)$$

where $i \in \{xy, xz, yz\}$, $k \in \{1, \dots, \tau_f\}$ is the timestep of autoregressive forecasting, and $Q_{s_i}^{t+k}$ is the learnable query at timestep $t+k$ in the i -th plane.

Since we have pre-trained the triplane occupancy representations, the future triplane can be used as the ground truth (GT) to supervise T³Former. Additionally, as we predict each plane independently, misalignments may occur. We finetune Φ_{dec} to align predictions of each plane. Formally:

$$J_{\text{fut}} = \mathbb{E}_{t,k,i}[\mathcal{L}_{\text{fut}}(\hat{s}_i^{t+k}, s_i^{t+k}) + \xi \mathcal{L}_{\text{occ}}(\hat{S}^{t+k}, S^{t+k})], \quad (9)$$

where \mathcal{L}_{fut} is the weighted sum of L1 and L2 losses, defined as $\mathcal{L}_{\text{fut}} = \mathcal{L}_1 + \gamma \mathcal{L}_2$, and γ, ξ are trade-off weights.

3.3 Motion planning with T³Former

Given the predicted scene changes, $\Delta \hat{s}^{t+k}$, provided by T³Former, we can generate a comprehensive motion plan by anticipating potential dangers based on both the scene changes and the previous and next scenes.

To achieve this, we first map the previous frame triplane \hat{s}^{t+k-1} , the triplane change $\Delta \hat{s}^{t+k}$, and the next frame triplane \hat{s}^{t+k} through the ResNet-18 networks [11] θ_p , θ_Δ , and θ_f , respectively, into a shared latent space, denoted as z^{t+k-1} , Δz^{t+k} , and z^{t+k} . Then, Δz^{t+k} passes through two independent fully connected (FC) layers and Sigmoid layers, collectively referred to as ζ_p and ζ_f , to generate the query vectors f^{t+k-1}

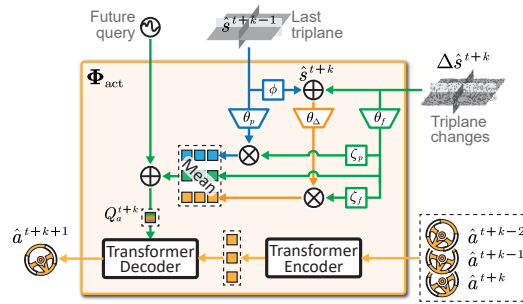


Figure 5: Motion planning with T³Former.

and f^{t+k} , which are then multiplied with z^{t+k-1} and z^{t+k} to obtain the motion-related features of the scene change relative to the last triplane and the next triplane. Finally, the motion-related features and the scene change Δz^{t+k} are element-wise averaged and processed through a FC layer, and then added to the future position encoding, resulting in the query variable for the next timestep motion plan, $Q_a^{t+k} \in \mathbb{R}^{d_{\text{act}}}$.

Next, we project the actions of the historical τ_p frames into the same dimension as Q_a^{t+k} , and employ a Transformer encoder to capture the motion dependencies within these frames. Then, Q_a^{t+k} is used in the Transformer decoder via cross-attention to predict the next action \hat{a}^{t+k+1} . The autoregressive generation of motion plans is defined as:

$$\hat{a}^{t+k+1} = \Phi_{\text{act}}(\hat{a}^{t+k-\tau_p:t+k}, \hat{s}^{t+k-1}, \Delta \hat{s}^{t+k}, Q_a^{t+k}). \quad (10)$$

Unlike OccWorld [58], we do not require an additional ego token to continuously track the agent’s motion trajectory. Instead, we can learn future motion directly from the scene changes and historical motion, as shown in Figure 5.

The optimization objective is defined as follows:

$$J_{\text{act}} = \mathbb{E}_{t,k}[\mathcal{L}_{\text{act}}(\hat{a}^{t+k}, a^{t+k})], \quad (11)$$

where \mathcal{L}_{act} measures the L2 discrepancy between the predicted and GT trajectories.

4 Experiments

4.1 Experimental settings

Targets and evaluation metrics. OWMs focus on jointly modeling occupancy forecasting and motion planning. Following the conventions in [58, 51, 46], we use the past four frames (2 seconds) to predict the outcomes of the next six frames (3 seconds). We conduct two sets of experiments:

- To validate the accuracy of 4D occupancy forecasting, we use intersection over union (IoU) and mean IoU (mIoU) across all semantic classes to measure the predicted future occupancy under the Occ3D dataset [39].
- To assess the precision and safety of motion planning, we calculate the L2 distance (in meters) between the planned and GT trajectories, and the collision rate with traffic participants’ bounding boxes using the nuScenes dataset [3].

Implementation details. The dataset consists of 1,000 scenes, of which 850 are used for training and 100 for testing. Each scene contains up to 40 timesteps, with a sampling frequency of 2Hz. The dimensions of the occupancy data S^t at each timestep are $16 \times 200 \times 200$. The pre-trained Triplane shape is $16 \times 100 \times 100$ with 8 channels. In Φ_{fut} , predictions for each plane incorporate features at $V = 5$ different scales, while the token dimension in Φ_{act} is $d_{\text{act}} = 50$. The objectives, $J_{\text{enc,dec}}$, J_{fut} , and J_{mot} , are optimized using AdamW with a weight regularization factor of 0.01, an initial learning rate of 0.001, and cosine decay with a minimum learning rate of 10^{-6} . We first pre-train Φ_{enc} and Φ_{dec} with a batch size of 10, using random flip augmentation to obtain the triplane representations. Then, we train Φ_{fut} and Φ_{act} with a batch size of 1, while fine-tuning Φ_{dec} . All training and testing are performed on 4 RTX 4090 GPUs. More details are provided in the supplementary material.

4.2 Comparisons with the state-of-the-art

4.2.1 4D occupancy forecasting

Table 1 presents the performance results of various methods, considering two modes of operation: (i) using 3D occupancy GTs as historical input, marked with “-O”; (ii) using predicted 3D occupancy data from FB-Occ [27] as historical input, marked with “-F”. “Copy&Paste” refers to directly using the GT occupancy data from the current timestep as predictions for future outcomes.

It is clear that SOTA methods’ Φ_{enc} fail to achieve high-fidelity compression, resulting in low reconstruction accuracy at time 0s. In contrast, both T³Former-O and T³Former-F utilize triplane representations that preserve both geometric and semantic information, leading to the highest mIoU and IoU reconstruction accuracy. This significantly aids in Φ_{fut} for predicting the next 3 seconds, effectively reducing error accumulation. Specifically, the “Copy&Paste” method, as a simple baseline, demonstrates substantial error accumulation. In contrast, T³Former-O shows a significant reduction in error, as indicated by mIoU and IoU averages. Notably, IoU generally surpasses mIoU, as predicting occupancy (whether occupied or unoccupied) is relatively straightforward, while semantic tracking without instance-level supervision is more challenging and prone to drift over time.

Table 1: Testing performance comparison with SOTA methods on the 4D occupancy forecasting task. Best values in each metric are **bolded**. 0s refers to reconstruction accuracy, while 1s, 2s, and 3s denote future prediction accuracy. Avg. is the average of 1s, 2s, and 3s.

Models	Input	mIoU (%) \uparrow					IoU (%) \uparrow				
		0s	1s	2s	3s	Avg.	0s	1s	2s	3s	Avg.
Copy&Paste	3D-Occ	66.38	14.91	10.54	8.52	11.33	62.29	24.47	19.77	17.31	20.52
OccWorld-O [58]	3D-Occ	66.38	25.78	15.14	10.51	17.14	62.29	34.63	25.07	20.18	26.63
OccLLaMA-O [46]	3D-Occ	75.20	25.05	19.49	15.26	19.93	63.76	34.56	28.53	24.41	29.17
RenderWorld [53]	3D-Occ	-	28.69	18.89	14.83	20.80	-	37.74	28.41	24.08	30.08
OccLLM-O [51]	3D-Occ	-	24.02	21.65	17.29	20.99	-	36.65	32.14	28.77	32.52
DOME-O [8]	3D-Occ	83.08	35.11	25.89	20.29	27.10	77.25	43.99	35.36	29.74	36.36
T ³ Former-O	3D-Occ	85.50	46.32	33.23	28.73	36.09	92.07	77.00	75.89	76.32	76.40
OccWorld-F [58, 27]	Camera	20.09	8.03	6.91	3.54	6.16	35.61	23.62	18.13	15.22	18.99
OccLLaMA-F [46, 27]	Camera	37.38	10.34	8.66	6.98	8.66	38.92	25.81	23.19	19.97	22.99
RenderWorld [53]	Camera	-	2.83	2.55	2.37	2.58	-	14.61	13.61	12.98	13.73
OccLLM-F [51, 27]	Camera	-	11.28	10.21	9.13	10.21	-	27.11	24.07	20.19	23.79
DOME-F [8]	Camera	75.00	24.12	17.41	13.24	18.25	74.31	35.18	27.90	23.44	28.84
T ³ Former-F [27]	Camera	43.52	24.87	18.30	15.63	19.60	54.31	38.98	37.45	31.89	36.11

4.2.2 Motion planning

We compare T³Former extensively with SOTA methods for autonomous driving, including LiDAR-based (IL [34], NMP [54], FF [13], EO [22]), camera-based (ST-P3 [14], UniAD [16], VAD [19], OccNet [40]), and occupancy-based methods (OccNet [40], OccWorld [58], RenderWorld [53], OccLLaMA [46]). The results are shown in Table 2.

Table 2: Testing performance of motion planning compared with SOTA method. Best and second-best values in each metric are **bolded** and underlined, respectively. Auxiliary supervision refers to additional supervision signals beyond the GT trajectories.

Models	Input	Auxiliary supervision	L2 (m) \downarrow				Collision rate (%) \downarrow			
			1s	2s	3s	Avg.	1s	2s	3s	Avg.
IL [34]	LiDAR	None	0.44	1.15	2.47	1.35	0.08	0.27	1.95	0.77
NMP [54]	LiDAR	Box+Motion	0.53	1.25	2.67	1.48	0.04	0.12	0.87	0.34
FF [13]	LiDAR	Freespace	0.55	1.20	2.54	1.43	0.06	0.17	1.07	0.43
EO [22]	LiDAR	Freespace	0.67	1.36	2.78	1.60	0.04	0.09	0.88	0.33
ST-P3 [14]	Camera	Map+Box+Depth	1.33	2.11	2.90	2.11	0.23	0.62	1.27	0.71
UniAD [16]	Camera	Map+Box+Motion+Track+Occ	0.48	<u>0.96</u>	1.65	<u>1.03</u>	0.05	0.17	0.71	<u>0.31</u>
VAD [19]	Camera	Map+Box+Motion	0.54	1.15	1.98	1.22	0.04	0.39	1.17	0.53
OccNet [40]	Camera	Map+Box+3D-Occ	1.29	2.13	2.99	2.14	0.21	0.59	1.37	0.72
OccNet [40]	3D-Occ	Map+Box	1.29	2.31	2.98	2.25	0.20	0.56	1.30	0.69
OccWorld-O [58]	3D-Occ	None	0.43	1.08	1.99	1.17	0.07	0.38	1.35	0.60
RenderWorld [53]	3D-Occ	None	<u>0.35</u>	0.91	1.84	1.03	0.05	0.40	1.39	0.61
OccLLaMA-O [46]	3D-Occ	None	0.37	1.02	2.03	1.14	0.04	0.24	1.20	0.49
T ³ Former-O	3D-Occ	None	0.32	0.91	<u>1.76</u>	1.00	0.08	0.32	0.51	0.30

Specifically, LiDAR- and camera-based methods explore various combinations of auxiliary supervisions to enhance the quality of planned motion trajectories. Despite their success, the auxiliary information they rely on is labor-intensive to obtain. In contrast, occupancy-based methods generate motion proposals using only occupancy representations. T³Former achieves the lowest L2 error over time, the lowest collision rate at the final time step, and the lowest average collision rate across all future motions. Compared to SOTA occupancy-based methods, T³Former shows excellent short-term and long-term planning (0s and 3s). This is primarily because we can establish precise, task-relevant correlations between scene changes and motion trajectories in a deep latent space, effectively filtering out noise from scene variations.

4.3 Visualizations

Comparisons with SOTA.

Figure 6 illustrates the evolution of the scene over the next 3 seconds, along with the corresponding motion predictions for two different scenarios. (i) In the first case, it is clear that OccWorld-O incorrectly labels the truck as a trailer initially, resulting in a continuous accumulation of errors. In contrast, T³Former effectively learns the motion dynamics of all objects in the scene, consistently tracking each vehicle over a long horizon, while providing clearer object boundaries. (ii) In the second

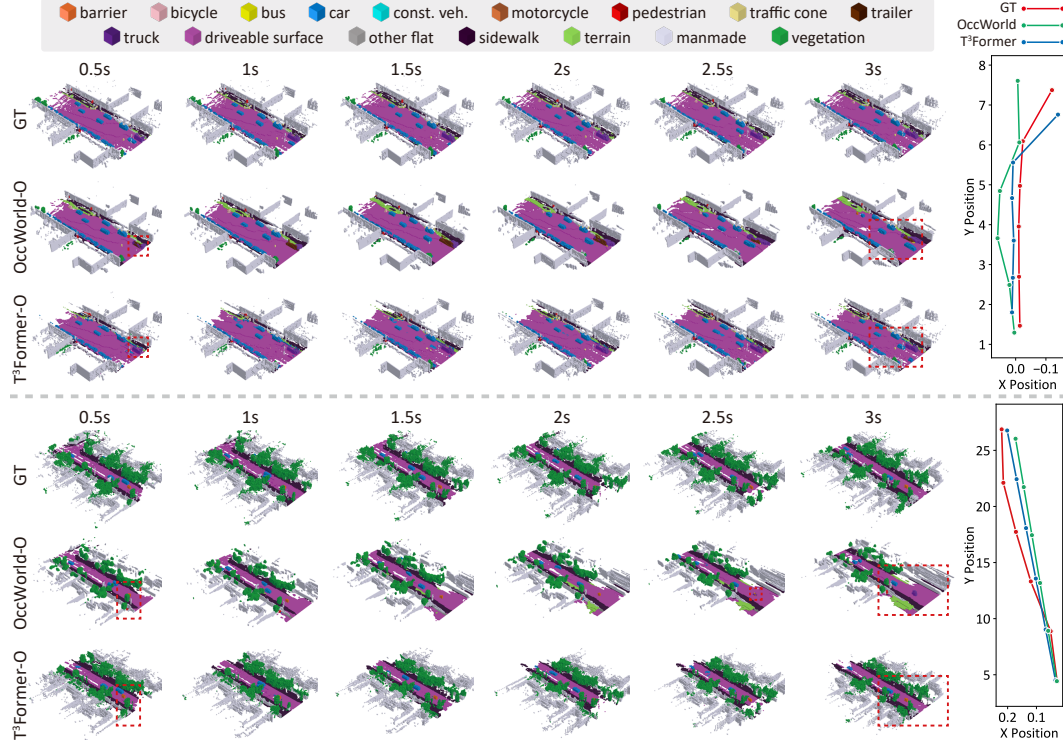


Figure 6: Visualization of 4D occupancy forecasting and motion planning for the next 3 seconds on the Occ3D test dataset (zoom in for a clearer view).

case, as the prediction horizon extends, OccWorld-O’s road boundary gradually fades, losing its clarity, whereas our method maintains the boundary shape of the road, including the trees. Additionally, OccWorld-O misidentifies the motorcycle as a truck at both 2.5s and 3s, while T³Former-O ensures that the semantics of small objects remain accurate over time. (iii) Under both scenarios, T³Former-O enables precise long-term future predictions, allowing our motion planning to rely solely on the evolving scene dynamics. This leads to more accurate trajectories and better avoidance of potential future hazards.

Driving view generation. Recent diffusion-based autonomous driving models [44, 7, 45] typically use historical driving views as conditions to generate future views. In contrast, our approach uses only triplane data as a lightweight condition. We fine-tune the diffusion model with ControlNet [56]. Figure 7 showcases synthetic images generated with different weather prompts and different triplane conditions. Triplane provides accurate 3D structural information, thereby enhancing consistency between pixel positions and semantics in the resulting synthetic 2D images.

Comparison of motion prediction. Figure 8 compares occupancy predictions for the three furthest frames in the prediction window, focusing on dynamic objects of varying sizes (cars and pedestrians) from a BEV perspective. Two reference lines are displayed to reflect

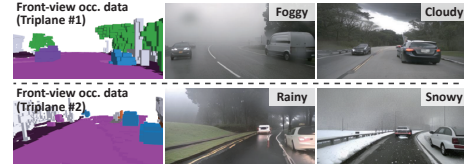


Figure 7: Driving view generations conditioned on different weather prompts and different triplane constraints.

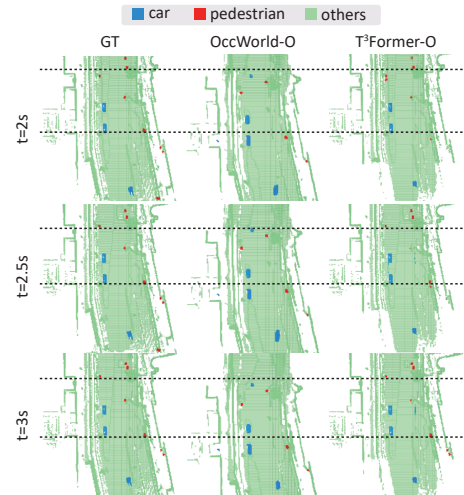


Figure 8: Predicted locations of dynamic objects for the three last frames.

the errors between the predictions and GT. The results of our method match the GT significantly better than OccWorld-O, which exhibits substantial drift. For instance, the predictions for the pedestrians at the top and the vehicle on the left clearly demonstrate this improvement

Limitation. As shown in Figure 9, T³Former produces sparse predictions in boundary regions. This is primarily due to occlusions in the original occupancy data, coupled with the use of triplanes that employ the orthogonal decomposition strategy [25, 17] to encode fine-grained geometric details. While this approach is effective for detailed representation, it complicates the task of correlating surrounding context and filling in the sparse areas during forecasting. In contrast, OccWorld tends to smooth and homogenize these sparse regions, a result of the inherent blurring issue in VAE-based models [5, 12]. In future work, we aim to improve content generation in these sparsely observed regions.

4.4 Ablation study

Table 3 validates the effectiveness of the key designs in T³Former. **M0** represents our complete version. For fairness, all ablation models are derived by replacing specific modules in **M0**, as outlined below: **M1** directly learns triplanes and downstream tasks (Eqs. (9) and (11)) in an end-to-end manner, without pre-training, leading to reduced encoder efficiency and performance degradation. **M2** replaces T³Former’s input with the VQ-VAE token from OccWorld [58], causing some geometric information loss. **M3** predicts the entire future triplane instead of Δ changes, showing that change prediction is more efficient. **M4** uses a single-scale Transformer to model temporal dynamics, failing to capture multi-scale object motion and causing error accumulation. **M5** predicts all future outcomes in parallel, resulting in poor performance due to the inability to correct autoregressive errors.

Table 4 analyzes the effect of different hyperparameters. ■ denotes our trade-off version. The **H1** series illustrates the impact of different latent shapes of triplanes. The setting refers to the number of channels, as well as the (height, width, and length). It is clear that increasing the spatial shape significantly enhances future prediction performance, while larger channel numbers provide little benefit and may even reduce performance. This is due to the introduction of feature redundancy, which complicates self-attention learning during forecasting. In the **H2** series, the setting defines the number of scales, Transformer layers, and self-attention heads in T³Former. Our results show that even a lightweight Transformer effectively captures key patterns, while increasing model size brings little benefit but adds computational overhead. Consequently, our design uses only 55M parameters – 23% fewer than OccWorld’s 72M – yet achieves superior efficiency. As illustrated in Figure 2, T³Former runs at 26 FPS on an RTX 4090 GPU, outperforming OccWorld’s 18 FPS.

5 Conclusion

This paper presents T³Former, a new 4D occupancy world model with three key designs: (i) pre-trained triplane representations for OWM, (ii) multi-scale Transformers for capturing motion dynamics, and (iii) triplane change prediction for occupancy forecasting and motion planning. T³Former achieves SOTA performance in 4D occupancy forecasting and motion planning with real-time capability. Our future work will dive deeper into driving view generation (see Figure 7), focusing on the synergy between prompt constraints, image texture, and temporal consistency in occupancy data.

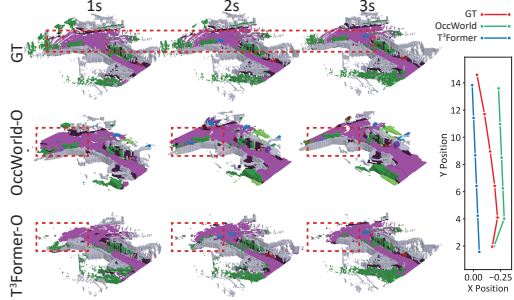


Figure 9: Limitations in sparse boundary regions.

Table 3: Ablation study of T³Former.

Idx.	Models	Avg. mIoU \uparrow	Avg. L2 \downarrow	FPS \uparrow
M0	T ³ Former-O	36.09	1.00	26
M1	w/o pretraining	33.96	1.17	26
M2	w/o triplane	28.97	1.10	21
M3	w/o triplane changes	30.51	1.04	27
M4	w/o multi-scale mot.	31.92	1.12	36
M5	w/o autoregression	34.65	1.06	34

Table 4: Effect of different hyperparameters.

Idx.	Setting	Avg. mIoU \uparrow	Avg. L2 \downarrow	FPS \uparrow
H1.1	8, (8, 50, 50)	26.78	1.33	37
H1.2	8, (16, 50, 50)	28.91	1.23	33
H1.3	8, (8, 100, 100)	31.42	1.17	30
H1.4	8, (16, 100, 100)	36.09	1.00	26
H1.5	16, (16, 100, 100)	36.20	1.09	23
H1.6	32, (16, 100, 100)	35.71	1.11	18
H2.1	$V = 3, (4, 16)$	35.91	1.08	28
H2.2	$V = 5, (4, 16)$	36.09	1.00	26
H2.3	$V = 5, (4, 32)$	36.14	1.04	21
H2.4	$V = 5, (8, 16)$	36.18	1.02	23
H2.5	$V = 7, (4, 16)$	35.65	0.98	20

References

- [1] Maxim Berman, Amal Rannen Triki, and Matthew B Blaschko. The lovász-softmax loss: A tractable surrogate for the optimization of the intersection-over-union measure in neural networks. In *Proceedings of the IEEE conference on computer vision and pattern recognition*, pages 4413–4421, 2018.
- [2] Tom Brown, Benjamin Mann, Nick Ryder, Melanie Subbiah, Jared D Kaplan, Prafulla Dhariwal, Arvind Neelakantan, Pranav Shyam, Girish Sastry, Amanda Askell, et al. Language models are few-shot learners. *Advances in neural information processing systems*, 33:1877–1901, 2020.
- [3] Holger Caesar, Varun Bankiti, Alex H Lang, Sourabh Vora, Venice Erin Liong, Qiang Xu, Anush Krishnan, Yu Pan, Giancarlo Baldan, and Oscar Beijbom. nuscenes: A multimodal dataset for autonomous driving. In *Proceedings of the IEEE/CVF conference on computer vision and pattern recognition*, pages 11621–11631, 2020.
- [4] Junliang Chen, Huaiyuan Xu, Yi Wang, and Lap-Pui Chau. Occprophet: Pushing efficiency frontier of camera-only 4d occupancy forecasting with observer-forecaster-refiner framework. In *ICLR*, 2025.
- [5] Dooseop Choi and KyoungWook Min. Hierarchical latent structure for multi-modal vehicle trajectory forecasting. In *European conference on computer vision*, pages 129–145. Springer, 2022.
- [6] Tuo Feng, Wenguan Wang, and Yi Yang. A survey of world models for autonomous driving. *arXiv preprint arXiv:2501.11260*, 2025.
- [7] Shenyuan Gao, Jiazhi Yang, Li Chen, Kashyap Chitta, Yihang Qiu, Andreas Geiger, Jun Zhang, and Hongyang Li. Vista: A generalizable driving world model with high fidelity and versatile controllability. *Advances in Neural Information Processing Systems*, 37:91560–91596, 2025.
- [8] Songen Gu, Wei Yin, Bu Jin, Xiaoyang Guo, Junming Wang, Haodong Li, Qian Zhang, and Xiaoxiao Long. Dome: Taming diffusion model into high-fidelity controllable occupancy world model. *arXiv preprint arXiv:2410.10429*, 2024.
- [9] David Ha and Jürgen Schmidhuber. Recurrent world models facilitate policy evolution. *Advances in neural information processing systems*, 31, 2018.
- [10] David Ha and Jürgen Schmidhuber. World models. *arXiv preprint arXiv:1803.10122*, 2018.
- [11] Kaiming He, Xiangyu Zhang, Shaoqing Ren, and Jian Sun. Deep residual learning for image recognition. In *Proceedings of the IEEE conference on computer vision and pattern recognition*, pages 770–778, 2016.
- [12] Irina Higgins, Loic Matthey, Arka Pal, Christopher Burgess, Xavier Glorot, Matthew Botvinick, Shakir Mohamed, and Alexander Lerchner. beta-vae: Learning basic visual concepts with a constrained variational framework. In *International conference on learning representations*, 2017.
- [13] Peiyun Hu, Aaron Huang, John Dolan, David Held, and Deva Ramanan. Safe local motion planning with self-supervised freespace forecasting. In *Proceedings of the IEEE/CVF Conference on Computer Vision and Pattern Recognition*, pages 12732–12741, 2021.
- [14] Shengchao Hu, Li Chen, Penghao Wu, Hongyang Li, Junchi Yan, and Dacheng Tao. St-p3: End-to-end vision-based autonomous driving via spatial-temporal feature learning. In *European Conference on Computer Vision*, pages 533–549. Springer, 2022.
- [15] Tao Hu, Xiaogang Xu, Ruihang Chu, and Jiaya Jia. Trivol: Point cloud rendering via triple volumes. In *Proceedings of the IEEE/CVF Conference on Computer Vision and Pattern Recognition*, pages 20732–20741, 2023.
- [16] Yihan Hu, Jiazhi Yang, Li Chen, Keyu Li, Chonghao Sima, Xizhou Zhu, Siqi Chai, Senyao Du, Tianwei Lin, Wenhai Wang, et al. Planning-oriented autonomous driving. In *Proceedings of the IEEE/CVF conference on computer vision and pattern recognition*, pages 17853–17862, 2023.
- [17] Yuanhui Huang, Wenzhao Zheng, Yunpeng Zhang, Jie Zhou, and Jiwen Lu. Tri-perspective view for vision-based 3d semantic occupancy prediction. In *Proceedings of the IEEE/CVF conference on computer vision and pattern recognition*, pages 9223–9232, 2023.
- [18] Fan Jia, Weixin Mao, Yingfei Liu, Yucheng Zhao, Yuqing Wen, Chi Zhang, Xiangyu Zhang, and Tiancai Wang. Adriver-i: A general world model for autonomous driving. *arXiv preprint arXiv:2311.13549*, 2023.
- [19] Bo Jiang, Shaoyu Chen, Qing Xu, Bencheng Liao, Jiajie Chen, Helong Zhou, Qian Zhang, Wenyu Liu, Chang Huang, and Xinggang Wang. Vad: Vectorized scene representation for efficient autonomous driving. In *Proceedings of the IEEE/CVF International Conference on Computer Vision*, pages 8340–8350, 2023.

- [20] Yuming Jiang, Shuai Yang, Tong Liang Koh, Wayne Wu, Chen Change Loy, and Ziwei Liu. Text2performer: Text-driven human video generation. In *Proceedings of the IEEE/CVF International Conference on Computer Vision*, pages 22747–22757, 2023.
- [21] Rajaei Khatib and Raja Giryes. Trinerflet: A wavelet based triplane nerf representation. In *European Conference on Computer Vision*, pages 358–374. Springer, 2024.
- [22] Tarasha Khurana, Peiyun Hu, Achal Dave, Jason Ziglar, David Held, and Deva Ramanan. Differentiable raycasting for self-supervised occupancy forecasting. In *European Conference on Computer Vision*, pages 353–369. Springer, 2022.
- [23] Tarasha Khurana, Peiyun Hu, David Held, and Deva Ramanan. Point cloud forecasting as a proxy for 4d occupancy forecasting. In *Proceedings of the IEEE/CVF Conference on Computer Vision and Pattern Recognition*, pages 1116–1124, 2023.
- [24] Diederik P Kingma, Max Welling, et al. Auto-encoding variational bayes, 2013.
- [25] Jumin Lee, Sebin Lee, Changho Jo, Woobin Im, Juhyeong Seon, and Sung-Eui Yoon. Semcity: Semantic scene generation with triplane diffusion. In *Proceedings of the IEEE/CVF conference on computer vision and pattern recognition*, pages 28337–28347, 2024.
- [26] Jinke Li, Xiao He, Chonghua Zhou, Xiaoqiang Cheng, Yang Wen, and Dan Zhang. Viewformer: Exploring spatiotemporal modeling for multi-view 3d occupancy perception via view-guided transformers. In *European Conference on Computer Vision*, pages 90–106. Springer, 2024.
- [27] Zhiqi Li, Zhiding Yu, David Austin, Mingsheng Fang, Shiyi Lan, Jan Kautz, and Jose M Alvarez. FB-OCC: 3D occupancy prediction based on forward-backward view transformation. *arXiv:2307.01492*, 2023.
- [28] Rui Liu, Wenguan Wang, and Yi Yang. Volumetric environment representation for vision-language navigation. In *Proceedings of the IEEE/CVF Conference on Computer Vision and Pattern Recognition*, pages 16317–16328, 2024.
- [29] Shaoyu Liu, Jianing Li, Guanghui Zhao, Yunjian Zhang, Xin Meng, Fei Richard Yu, Xiangyang Ji, and Ming Li. Eventgpt: Event stream understanding with multimodal large language models. *arXiv preprint arXiv:2412.00832*, 2024.
- [30] Fan Lu, Guang Chen, Zhijun Li, Lijun Zhang, Yinlong Liu, Sanqing Qu, and Alois Knoll. Monet: Motion-based point cloud prediction network. *IEEE Transactions on Intelligent Transportation Systems*, 23(8): 13794–13804, 2021.
- [31] Junyi Ma, Xieyuanli Chen, Jiawei Huang, Jingyi Xu, Zhen Luo, Jintao Xu, Weihao Gu, Rui Ai, and Hesheng Wang. Cam4docc: Benchmark for camera-only 4d occupancy forecasting in autonomous driving applications. In *Proceedings of the IEEE/CVF Conference on Computer Vision and Pattern Recognition*, pages 21486–21495, 2024.
- [32] Qihang Ma, Xin Tan, Yanyun Qu, Lizhuang Ma, Zhizhong Zhang, and Yuan Xie. Cotr: Compact occupancy transformer for vision-based 3d occupancy prediction. In *Proceedings of the IEEE/CVF Conference on Computer Vision and Pattern Recognition*, pages 19936–19945, 2024.
- [33] Benedikt Mersch, Xieyuanli Chen, Jens Behley, and Cyrill Stachniss. Self-supervised point cloud prediction using 3d spatio-temporal convolutional networks. In *Conference on Robot Learning*, pages 1444–1454. PMLR, 2022.
- [34] Nathan D Ratliff, J Andrew Bagnell, and Martin A Zinkevich. Maximum margin planning. In *Proceedings of the 23rd international conference on Machine learning*, pages 729–736, 2006.
- [35] Ali Razavi, Aaron Van den Oord, and Oriol Vinyals. Generating diverse high-fidelity images with vq-vae-2. *Advances in neural information processing systems*, 32, 2019.
- [36] Olaf Ronneberger, Philipp Fischer, and Thomas Brox. U-net: Convolutional networks for biomedical image segmentation. In *Medical image computing and computer-assisted intervention—MICCAI 2015: 18th international conference, Munich, Germany, October 5-9, 2015, proceedings, part III 18*, pages 234–241. Springer, 2015.
- [37] J Ryan Shue, Eric Ryan Chan, Ryan Po, Zachary Ankner, Jiajun Wu, and Gordon Wetzstein. 3d neural field generation using triplane diffusion. In *Proceedings of the IEEE/CVF Conference on Computer Vision and Pattern Recognition*, pages 20875–20886, 2023.

- [38] Luchuan Song, Pinxin Liu, Lele Chen, Guojun Yin, and Chenliang Xu. Tri 2-plane: Thinking head avatar via feature pyramid. In *European Conference on Computer Vision*, pages 1–20. Springer, 2024.
- [39] Xiaoyu Tian, Tao Jiang, Longfei Yun, Yucheng Mao, Huitong Yang, Yue Wang, Yilun Wang, and Hang Zhao. Occ3d: A large-scale 3d occupancy prediction benchmark for autonomous driving. *Advances in Neural Information Processing Systems*, 36:64318–64330, 2023.
- [40] Wenwen Tong, Chonghao Sima, Tai Wang, Li Chen, Silei Wu, Hanming Deng, Yi Gu, Lewei Lu, Ping Luo, Dahua Lin, et al. Scene as occupancy. In *Proceedings of the IEEE/CVF International Conference on Computer Vision*, pages 8406–8415, 2023.
- [41] Aaron Van Den Oord, Oriol Vinyals, et al. Neural discrete representation learning. *Advances in neural information processing systems*, 30, 2017.
- [42] Ashish Vaswani, Noam Shazeer, Niki Parmar, Jakob Uszkoreit, Llion Jones, Aidan N Gomez, Łukasz Kaiser, and Illia Polosukhin. Attention is all you need. *Advances in neural information processing systems*, 30, 2017.
- [43] Jiabao Wang, Zhaojiang Liu, Qiang Meng, Liujiang Yan, Ke Wang, Jie Yang, Wei Liu, Qibin Hou, and Ming-Ming Cheng. Opus: occupancy prediction using a sparse set. *arXiv preprint arXiv:2409.09350*, 2024.
- [44] Xiaofeng Wang, Zheng Zhu, Guan Huang, Xinze Chen, Jiagang Zhu, and Jiwen Lu. Drivedreamer: Towards real-world-drive world models for autonomous driving. In *European Conference on Computer Vision*, pages 55–72. Springer, 2024.
- [45] Yuqi Wang, Jiawei He, Lue Fan, Hongxin Li, Yuntao Chen, and Zhaoxiang Zhang. Driving into the future: Multiview visual forecasting and planning with world model for autonomous driving. In *Proceedings of the IEEE/CVF Conference on Computer Vision and Pattern Recognition*, pages 14749–14759, 2024.
- [46] Julong Wei, Shanshuai Yuan, Pengfei Li, Qingda Hu, Zhongxue Gan, and Wenchao Ding. Oc-llama: An occupancy-language-action generative world model for autonomous driving. *arXiv preprint arXiv:2409.03272*, 2024.
- [47] Yi Wei, Linqing Zhao, Wenzhao Zheng, Zheng Zhu, Jie Zhou, and Jiwen Lu. Surroundocc: Multi-camera 3d occupancy prediction for autonomous driving. In *Proceedings of the IEEE/CVF International Conference on Computer Vision*, pages 21729–21740, 2023.
- [48] Zehuan Wu, Jingcheng Ni, Xiaodong Wang, Yuxin Guo, Rui Chen, Lewei Lu, Jifeng Dai, and Yuwen Xiong. Holodrive: Holistic 2d-3d multi-modal street scene generation for autonomous driving. *arXiv preprint arXiv:2412.01407*, 2024.
- [49] Haoran Xu, Peixi Peng, Xinyi Zhang, Guang Tan, Yaokun Li, Shuaixian Wang, and Luntong Li. Exploiting continuous motion clues for vision-based occupancy prediction. In *AAAI*, 2025.
- [50] Jingyi Xu, Xieyuanli Chen, Junyi Ma, Jiawei Huang, Jintao Xu, Yue Wang, and Ling Pei. Spatiotemporal decoupling for efficient vision-based occupancy forecasting. *arXiv preprint arXiv:2411.14169*, 2024.
- [51] Tianshuo Xu, Hao Lu, Xu Yan, Yingjie Cai, Bingbing Liu, and Yingcong Chen. Occ-llm: Enhancing autonomous driving with occupancy-based large language models. In *International Conference on Robotics and Automation*, 2025.
- [52] Xu Yan, Jiantao Gao, Jie Li, Ruimao Zhang, Zhen Li, Rui Huang, and Shuguang Cui. Sparse single sweep lidar point cloud segmentation via learning contextual shape priors from scene completion. In *Proceedings of the AAAI conference on artificial intelligence*, pages 3101–3109, 2021.
- [53] Ziyang Yan, Wenzhen Dong, Yihua Shao, Yuhang Lu, Liu Haiyang, Jingwen Liu, Haozhe Wang, Zhe Wang, Yan Wang, Fabio Remondino, et al. Renderworld: World model with self-supervised 3d label. In *International Conference on Robotics and Automation*, 2025.
- [54] Wenyuan Zeng, Wenjie Luo, Simon Suo, Abbas Sadat, Bin Yang, Sergio Casas, and Raquel Urtasun. End-to-end interpretable neural motion planner. In *Proceedings of the IEEE/CVF conference on computer vision and pattern recognition*, pages 8660–8669, 2019.
- [55] Hang Zhang, Anton Savov, and Benjamin Dillenburger. Maskplan: Masked generative layout planning from partial input. In *Proceedings of the IEEE/CVF Conference on Computer Vision and Pattern Recognition*, pages 8964–8973, 2024.

- [56] Lvmin Zhang, Anyi Rao, and Maneesh Agrawala. Adding conditional control to text-to-image diffusion models. In *Proceedings of the IEEE/CVF international conference on computer vision*, pages 3836–3847, 2023.
- [57] Yumeng Zhang, Shi Gong, Kaixin Xiong, Xiaoqing Ye, Xiao Tan, Fan Wang, Jizhou Huang, Hua Wu, and Haifeng Wang. Bevworld: A multimodal world model for autonomous driving via unified bev latent space. *arXiv preprint arXiv:2407.05679*, 2024.
- [58] Wenzhao Zheng, Weiliang Chen, Yuanhui Huang, Borui Zhang, Yueqi Duan, and Jiwen Lu. Occworld: Learning a 3d occupancy world model for autonomous driving. In *European conference on computer vision*, pages 55–72. Springer, 2024.
- [59] Gengze Zhou, Yicong Hong, and Qi Wu. Navgpt: Explicit reasoning in vision-and-language navigation with large language models. In *Proceedings of the AAAI Conference on Artificial Intelligence*, pages 7641–7649, 2024.